Journal: Monthly Notices of the Royal Astronomical Society
Article doi: 10.1093/mnras/stx968
Article title: Temporal intensity interferometry for characterization of very narrow spectral lines
First Author: P. K. Tan
Corr. Author: C. Kurtsiefer

INSTRUCTIONS

We encourage you to use Adobe's editing tools (please see the next page for instructions). If this is not possible, please list clearly in an e-mail. Please do not send corrections as track changed Word documents.

Changes should be corrections of typographical errors only. Changes that contradict journal style will not be made.

These proofs are for checking purposes only. They should not be considered as final publication format. The proof must not be used for any other purpose. In particular we request that you: do not post them on your personal/institutional web site, and do not print and distribute multiple copies. Neither excerpts nor all of the article should be included in other publications written or edited by yourself until the final version has been published and the full citation details are available. You will be sent these when the article is published.

1. **Licence to Publish:** Oxford Journals requires your agreement before publishing your article. If you haven't already completed this, please sign in with your My Account information and complete the online licence form. Details on how to do this can be found in the Welcome to Oxford Journals email.
2. **Permissions: Permission to reproduce any third party material in your paper should have been obtained prior to acceptance. If your paper contains figures or text that require permission to reproduce, please inform me immediately by email.**
3. **Author groups:** Please check that all names have been spelled correctly and appear in the correct order. Please also check that all initials are present. Please check that the author surnames (family name) have been correctly identified by a pink background. If this is incorrect, please identify the full surname of the relevant authors. Occasionally, the distinction between surnames and forenames can be ambiguous, and this is to ensure that the authors' full surnames and forenames are tagged correctly, for accurate indexing online.
4. **Figures:** If applicable, figures have been placed as close as possible to their first citation. Please check that they are complete and that the correct figure legend is present. Figures in the proof are low resolution versions that will be replaced with high resolution versions when the journal is printed.
5. **Missing elements:** Please check that the text is complete and that all figures, tables and their legends are included.
6. **Special characters and equations:** Please check that special characters, equations and units have been reproduced accurately.
7. **URLs:** Please check that all web addresses cited in the text, footnotes and reference list are up-to-date.
8. **Funding:** If applicable, any funding used while completing this work should be highlighted in the Acknowledgements section. Please ensure that you use the full official name of the funding body.

AUTHOR QUERIES - TO BE ANSWERED BY THE CORRESPONDING AUTHOR

The following queries have arisen during the typesetting of your manuscript. Please answer these queries by marking the required corrections at the appropriate point in the text.

Query No.	Nature of Query	Author's Response
Q1	Author: The figures have been processed according to the information you entered during the submission of your manuscript. Please note that there is a charge of £200 (+VAT) for publishing in colour in print. There is no charge to publish figures in black and white in print and in colour online. If you have already requested print colour figures or have now decided to have print colour figures please confirm that you are willing to pay the £200 (+VAT) charge. You will be invoiced upon publication. If you do not wish to have your figures published in colour in print, please confirm. Black and white versions of figures are provided at the end of the paper. Please check the black and white versions to assess their quality for the print version of the of the journal, please contact us if you have any concerns.	
Q2	Author: Please supply email addresses for between one and three authors who are willing to correspond with readers and for their email address to be included in the article	
Q3	Author: To check that we have your surnames correctly identified and tagged (e.g. for indexing), we have coloured pink the names that we have assumed are surnames. If any of these are wrong, please let us know so that we can amend the tagging.	
Q4	Author: If you refer to any data bases in your paper, please note the journal policy for properly crediting those responsible for compiling the data base. Rather than citing only a URL, if at all possible please also cite a reference (and include it in the reference list), or if a reference is not available then the names of those who compiled the data base. Note that some data bases do provide guidelines on how they should be cited – please check for these and follow them in your paper where appropriate.	
Q5	Author: The MNRAS list of approved key words has been revised and updated. The new list is appended to these proofs. If you had previously selected key words from the old list, please now check them carefully against the new list in case they need to be changed, or there are new ones that you would like to add. If you had not previously selected key words from the MNRAS approved list, please now choose up to six from the new list.	
Q6	Author: When used to mean the numerical value '3.14', the Greek letter 'pi' must always be written in roman (i.e. 'π' rather than 'π'). Please check all the notations throughout the text carefully.	
Q7	Author: Please check the figures in the PDF proof carefully.	
Q8	Author: As per journal style, the running head short title of a paper must not exceed 45 characters (including spaces between words and punctuation marks); please supply an alternative short title of up to 45 characters (including any spaces between words and punctuation marks) that can be used instead.	

Query No.	Nature of Query	Author's Response
Q9	Author: The article 'a' preceding the listed acronym (SNR) has been changed to 'an' throughout the text because we are assuming this acronym is read as its individual letters and not as the entire word.	
Q10	Author: In order to validate your funding information prior to publication, please check and confirm whether the name of the funding body given in your manuscript is complete and correct. If any edits are required please mark them on the text. Please also expand any acronyms used in this section. If multiple grants are cited, please ensure the text of your funding statement clearly indicates which grant applies to which funding body.	
Q11	Author: Please provide the volume number or page number (whichever is applicable) in this reference.	
Q12	Author: Please list all the authors if eight or fewer. Also, please provide the volume number or page number (whichever is applicable) in this reference.	
Q13	Author: Please list all the authors if eight or fewer. Also, please provide the volume number or page number (whichever is applicable) in this reference.	
Q14	Author: Please provide the volume number or page number (whichever is applicable) in this reference. Also, please check the journal title and correct if necessary.	
Q15	Author: Please check the journal title and provide the full name of this journal.	
Q16	Author: Please provide the volume number or page number (whichever is applicable) in this reference.	
Q17	Author: Please provide the volume number or page number (whichever is applicable) in this reference.	

MAKING CORRECTIONS TO YOUR PROOF

These instructions show you how to mark changes or add notes to your proofs using Adobe Acrobat Professional versions 7 and onwards, or Adobe Reader DC. To check what version you are using go to **Help** then **About**. The latest version of Adobe Reader is available for free from get.adobe.com/reader.

DISPLAYING THE TOOLBARS

Adobe Reader DC

In Adobe Reader DC, the Comment toolbar can be found by clicking 'Comment' in the menu on the right-hand side of the page (shown below).

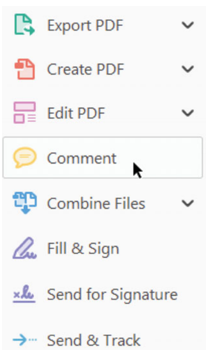

The toolbar shown below will then display along the top.

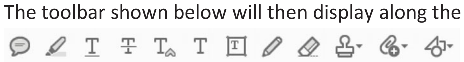

Acrobat Professional 7, 8, and 9

In Adobe Professional, the Comment toolbar can be found by clicking 'Comment(s)' in the top toolbar, and then clicking 'Show Comment & Markup Toolbar' (shown below).

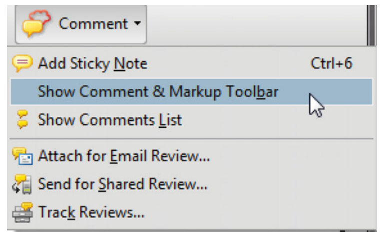

The toolbar shown below will then be displayed along the top.

USING TEXT EDITS AND COMMENTS IN ACROBAT

This is the quickest, simplest and easiest method both to make corrections, and for your corrections to be transferred and checked.

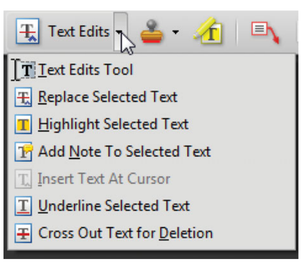

1. Click **Text Edits**
2. Select the text to be annotated or place your cursor at the insertion point and start typing.
3. Click the **Text Edits** drop down arrow and select the required action.

You can also right click on selected text for a range of commenting options, or add sticky notes.

SAVING COMMENTS

In order to save your comments and notes, you need to save the file (**File, Save**) when you close the document.

USING COMMENTING TOOLS IN ADOBE READER

All commenting tools are displayed in the toolbar. You cannot use text edits, however you can still use highlighter, sticky notes, and a variety of insert/replace text options.

POP-UP NOTES

In both Reader and Acrobat, when you insert or edit text a pop-up box will appear. In **Acrobat** it looks like this:

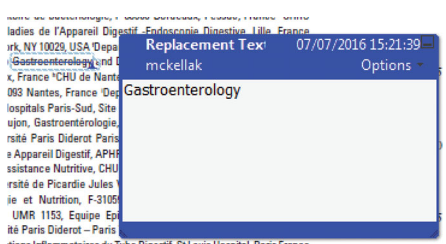

In **Reader** it looks like this, and will appear in the right-hand pane:

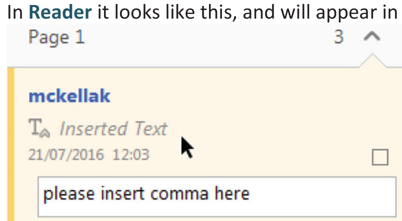

DO NOT MAKE ANY EDITS DIRECTLY INTO THE TEXT, USE COMMENTING TOOLS ONLY.

MNRAS (2017)
Advance Access publication 2017 April 24

doi:10.1093/mnras/stx968

Temporal intensity interferometry for characterization of very narrow spectral lines

P. K. Tan[1] and C. Kurtsiefer[1,2★]

[1]*Centre for Quantum Technologies, 3 Science Drive 2, 117543, Singapore*
[2]*Department of Physics, National University of Singapore, 2 Science Drive 3, 117551, Singapore*

Accepted 2017 April 20. Received 2017 April 20; in original form 2016 November 17

ABSTRACT

Some stellar objects exhibit very narrow spectral lines in the visible range additional to their blackbody radiation. Natural lasing has been suggested as a mechanism to explain narrow lines in Wolf–Rayet stars. However, the spectral resolution of conventional astronomical spectrographs is still about two orders of magnitude too low to test this hypothesis. We want to resolve the linewidth of narrow spectral emissions in starlight. A combination of spectral filtering with single-photon-level temporal correlation measurements breaks the resolution limit of wavelength-dispersing spectrographs by moving the linewidth measurement into the time domain. We demonstrate in a laboratory experiment that temporal intensity interferometry can determine a 20-MHz-wide linewidth of Doppler-broadened laser light and identify a coherent laser light contribution in a blackbody radiation background.

Key words: line: identification – instrumentation: interferometers – techniques: spectroscopic.

UNCORRECTED PROOF

1 NARROW EMISSION LINES AND ASTROPHYSICAL LASERS

Some spectral lines in the visible range emitted from stellar systems appear to be unusually narrow. Specifically, some emission lines from the Weigelt blobs in η Car, when observed with the *Hubble Space Telescope*, appeared to be limited by the instrument resolution of about 40 GHz, corresponding to velocity spreads of 25 km s^{-1} (Hamann & DePoy 1994; Zethson et al. 2012). Another example is the Wolf–Rayet progenitor SN2013cu, for which emission lines with relatively broad base of 2500 km s^{-1} full width at zero intensity were observed, on which narrow unresolved (instrument-limited at 150 km s^{-1}) lines are superimposed (Gal-Yam et al. 2014).

Such observations suggest very low temperatures of the emission medium, and trigger speculations on mechanisms like stimulated emission, which can lead to optical emission much narrower than the participating atomic or molecular transition. Following first laboratory demonstrations of maser and laser radiation and the detection of strong interstellar microwave emission from molecular gas clouds (Weaver et al. 1965), natural non-visible lasers from astrophysical sources were proposed to be responsible for such narrow emission lines (Menzel 1970; Varshni & Nasser 1986).

Natural stellar laser candidates in the visible range are suspected to have a spectral linewidth around 10 MHz (Johansson & Letokhov 2005), which would not even be resolvable by conventional astronomical spectrographs with a high resolution (10^5) like the Keck High Resolution Echelle Spectrometer (Griest et al. 2010). Therefore, alternative spectroscopical techniques like heterodyne spectroscopy (Hale et al. 2000; Sonnabend et al. 2005) or, as we investigate in this paper, temporal photon correlation spectroscopy may help to better understand the nature of these narrow emission lines. Temporal photon correlation spectroscopy is in widespread use in material science and fluorescence microscopy, where it is also referred to as dynamic light scattering and quasi-elastic light scattering, and used to characterize the particle distribution in suspensions (Saleh 1978; Becker 2005; Pike 2010). Application of this spectroscopy technique in astronomy seems less common (Dravins & Germanà 2008), but may be advantageous in characterizing narrow linewidths. Moreover, one may even be able to experimentally assess the presence of a natural lasing mechanism directly in the visible range , as we show in this work.

2 COMPARISON WITH OTHER SPECTROSCOPY TECHNIQUES

Modern astronomical echelle spectrographs have typical resolutions between 30 000 and 150 000 (Murphy et al. 2007) with the target starlight and reference calibration light (such as laser frequency combs) fed by multimode fibres, because starlight cannot be efficiently coupled to single-mode optical fibres in the visible regime (Wilken et al. 2012).

Optical homo- or heterodyning (Siegman 1966; Mandel & Wolf 1975) has the potential for a basically unlimited spectral resolution, but is conditional on the overlap of spatial modes between the

★ E-mail: phyck@nus.edu.sg

© 2017 The Authors
Published by Oxford University Press on behalf of the Royal Astronomical Society

input light with the local oscillator. While this can be accomplished in a lab environment using single-mode fibres, it is inefficient to couple starlight into optical single-mode fibres due to atmospheric turbulence and seeing (Fried 1967). Mode matching in a free space geometry for heterodyning is equally difficult for the same reason (Shaklan & Roddier 1988).

For Michelson interferometry or Fourier transform spectroscopy, which could be less sensitive to phase fluctuations, a resolution of tens of MHz would require scanning a path length difference over several metres in steps shorter than the optical wavelength (Loewenstein 1966; Sakai, Vanasse & Forman 1968) – a requirement that would be mechanically very challenging.

3 INTENSITY INTERFEROMETRY FOR TIME DOMAIN SPECTROSCOPY

Intensity interferometry was used to investigate the spatial coherence properties of starlight to infer their angular diameter (Hanbury-Brown & Twiss 1956), but first demonstration experiments were carried out on spectral lines from a Mercury gas discharge lamp (Hanbury-Brown & Twiss 1958). In essence, normalized intensity correlations

$$g^{(2)}(\tau) = \frac{\langle I(t)I(t+\tau)\rangle}{\langle I(t)\rangle^2} \tag{1}$$

are recorded as a function of the time difference τ by evaluating photodetection events from detectors observing the same light source. For stationary light of a single polarization, the normalized intensity correlation $g^{(2)}(\tau)$ is related to the normalized (electrical) field correlation $g^{(1)}(\tau)$ (Mandel & Wolf 1995) via

$$g^{(2)}(\tau) = 1 + |g^{(1)}(\tau)|^2 \,. \tag{2}$$

The Wiener–Khinchin theorem (Wiener 1930; Khinchin 1934) links the field correlation to the spectral power density *S*(*f*) through a Fourier transform $\mathcal{F}$:

$$S(f) \propto \mathcal{F}[g^{(1)}(\tau)] \,. \tag{3}$$

Therefore – within the limits of reconstructing the phase of the complex $g^{(1)}(\tau)$ from $g^{(2)}(\tau)$ via (2) – it is possible to extract information about the spectral power density *S*(*f*) of the light source from a measured intensity correlation $g^{(2)}(\tau)$. A narrow spectral distribution *S*(*f*) of width δf will result in a $g^{(2)}(\tau)$ with a characteristic time-scale $\tau_c \propto 1/\delta f$.

The width δf of narrow spectral lines can therefore be measured in the time domain overcoming the resolving power of wavelength-dispersive instruments like spectrographs or narrow-band interference filters. Note, however, that this does not allow determination of the absolute spectral position of a line, since a frequency shift
Q6 Δf of a narrow distribution results in a complex oscillating term $e^{2\pi i \Delta f \tau}$ in $g^{(1)}(\tau)$, but leaves $g^{(2)}(\tau)$ unchanged due to the modulus in (2).

In stellar light sources, narrow spectral lines tend to appear against a large background of blackbody radiation. A direct measurement of the second-order correlation function is therefore difficult, because the signal is dominated by the blackbody contribution with a very short coherence time in the order of 10^{-14} s. Therefore, adequate preliminary filtering has to suppress the thermal background to a level where time domain spectroscopy can be carried out. It is also necessary that the light exhibits some non-Poissonian intensity fluctuations, since for light with Poissonian statistics, e.g. coherent laser light, the intensity correlation is flat [$g^{(2)}(\tau) = 1$; Glauber 1963 and has no structure that would reveal any spectral properties.

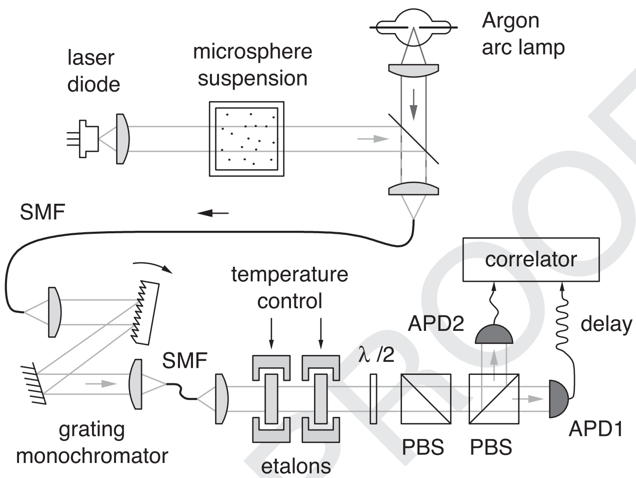

Figure 1. Experimental set-up. Light from a laser diode ($\lambda_L = 513.8$ nm) is Doppler-broadened by passing through a suspension of microspheres (0.2 μm diameter), combined with light from an Argon arc lamp on a microscope slide, and coupled into a single-mode optical fibre (SMF). The bottom part shows the analysis system, consisting of a grating monochromator and a temperature-tuned etalon pair to select a 3.2-GHz-wide spectral window around 513.8 nm from the composite light. Temporal photon pair correlations are recorded to identify different light contributions. PBS: polarizing beam splitter; $\lambda/2$: half wave plate; APD: single-photon avalanche photodetectors.

In this work, we simulate the characteristic spectrum of natural stellar laser candidates in the visible range by combining phase-randomized artificially Doppler-broadened laser light with spectrally wide blackbody radiation. We then characterize the narrow spectral line by time-resolved intensity interferometry after passing the composite light through a diffraction grating and two etalons to suppress the blackbody contribution.

4 EXPERIMENTAL SET-UP

Our experimental set-up is illustrated in Fig. 1. Composite test light is prepared by combining light from a laser diode (Osram PL520, $P = 50$ mW) at a wavelength of $\lambda_L = 513.8$ nm with blackbody radiation from an Argon arc lamp with an effective blackbody temperature of around 6000 K on an uncoated microscope glass slide. This combines approximately 4 per cent of the incident laser light with 92 per cent of the Argon arc lamp output, with another 4 per cent loss in the splitter due to the lack of antireflective coating. The resulting spectrum recorded with a grating spectrometer of approximately 0.12-nm resolution is shown in Fig. 2. Q7

The very narrow-band laser light is Doppler-broadened by passing it through a cuvette containing a suspension of standard monodisperse polystyrene microspheres of 0.2 μm diameter in water, following Dravins, Lagadec & Nuñez (2015). These microspheres serve as scattering centres undergoing Brownian motion at room temperature. The resultant phase randomization causes the laser light to exhibit pseudo-thermal photon bunching behaviour (Martienssen & Spiller 1964; Arecchi 1965; Scarl 1966, 1968; Estes, Narducci & Tuft 1971; Hard, Zeh & Allen 1977). The coherence properties of light leaving the suspension depend on the temperature of the suspension, the viscosity (ratio of water to microspheres) and beam focus (Dravins & Lagadec 2014); these parameters were not fully characterized, but a combination of a beam waist of roughly 1 mm, with beads-concentration of approximately

COLOUR ONLINE, B&W IN PRINT
UNCORRECTED PROOF

COLOUR ONLINE, B&W IN PRINT

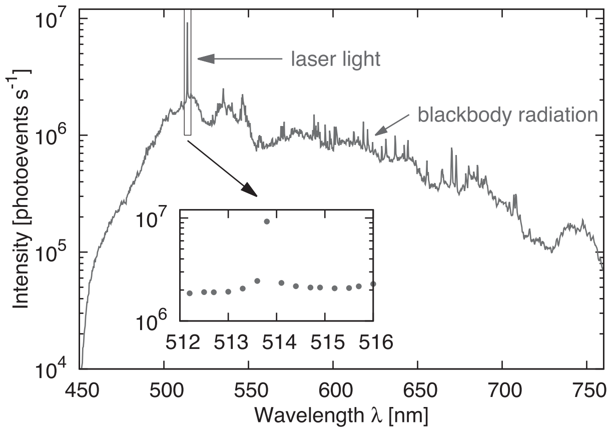

Figure 2. Spectrum of the test light source in Fig. 1 without Doppler broadening. The broad background over the whole visible range resembles blackbody radiation at an effective temperature of $T = 6000\,\mathrm{K}$, while the inset shows the unresolved spectrum around the laser line. The resolution of the spectrometer is about 0.12 nm.

0.1 per cent solids [weight/volume] at room temperature (23°C) lead to Doppler-broadened light we could investigate with our technique.

The microsphere suspension with its milky appearance reduces the intensity of the laser light by over two orders of magnitude, which is too low to allow proper identification against the blackbody radiation background in a spectral measurement with our grating spectrometer.

To identify the laser light admixture to the blackbody radiation, the test light is first coupled into a single-mode fibre (Thorlabs 460HP). After collimation, the light passes through a monochromator based on a reflective diffraction grating (1200 lines mm^{-1}, blazed for 500 nm). The monochromator is calibrated to the 546.1 nm line from a Mercury discharge lamp, where it shows a transmission bandwidth (full width at half-maximum, FWHM) of about 0.12 nm.

A second single-mode fibre enforces spatial coherence again, before the light passes through a pair of temperature-tuned plane-parallel solid etalons made of fused silica (Suprasil311) with a refractive index $n = 1.4616$ and coatings of a nominal reflectivity $R =$ [illegible] per cent at λ_L. This corresponds to an estimated finesse $\mathcal{F}_R = \pi\sqrt{R}/(1-R) = 63.9$. The etalons have thicknesses of $d_1 = 0.5$ mm and $d_2 = 0.3$ mm, corresponding to a free spectral range $\mathrm{FSR} = c/(2dn)$ of 205 and 342 GHz, respectively. Their temperatures are stabilized to overlap the transmission maxima at the laser wavelength. Both etalons, in conjunction with the diffraction grating, suppress most of the blackbody background (Tan et al. 2014), transmitting only an optical bandwidth $\delta f \approx \mathrm{FSR}_1/\mathcal{F}_R \approx 3.2\,\mathrm{GHz}$ (FWHM), corresponding to a coherence time $\tau_c = 1/\delta f \approx 0.31$ ns. This filter combination has an effective spectral resolving power of about 10^5, which is comparable to current astronomical spectrographs (Griest et al. 2010).

The filtered light is polarized by a first polarizing beam splitter (PBS), and distributed by a second PBS into a pair of actively quenched silicon avalanche photodetectors (APD) with a timing jitter of about 40 ps (Tan, Chan & Kurtsiefer 2016). Photodetection rates are balanced by rotating the first PBS that is preceded by a half wave plate to maximize the count rates. Coincidence photoevents are recorded using a fast digital oscilloscope. The photodetectors exhibit a dark count rate of 50 events s^{-1}, predominantly from the detector thermal noise, which is negligible in the subsequent coincidence measurements. The coincidence histograms were normalized to obtain a $g^{(2)}(\tau) = 1$ for large τ, because the oscilloscope had an unknown dead time for histogram processing that made a direct normalization impossible.

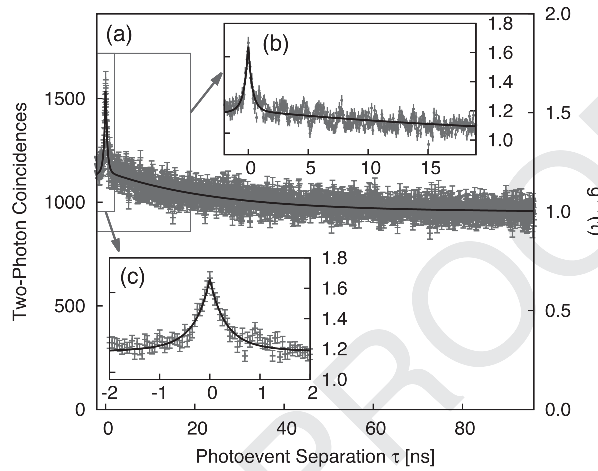

Figure 3. (a) The two-photoevent coincidence histogram from filtered blackbody radiation with a Doppler- broadened laser light contribution shows two exponential decays on a short and a long time-scale (bin width 50 ps). The solid line shows a fit of the data to model (8), assuming $f_B = f_L$. The two zooms show (b) an oscillatory behaviour on top of the slow decay and (c) a good match between the fit and measured data for the filtered blackbody radiation on a short time-scale.

5 IDENTIFYING EMISSION LINEWIDTH

In the first experiment, we want to measure the linewidth of the laser light that was Doppler-broadened by random scattering in the microsphere suspension on a background of blackbody radiation. Both broadened laser light and blackbody radiation resulted in about 2×10^4 photoevents per second each behind the filter stack formed by gratings, etalons and polarization filters.

The histogram of two-photon coincidences as a function of photodetection event separation τ is shown in Fig. 3, with a total of 2×10^6 coincidences recorded for -2 ns $< \tau <$ 96 ns. For time differences $|\tau| < 1$ ns, the sharp peak due to filtered blackbody radiation is visible, while on a longer time-scale, the Doppler-broadened laser contribution due to phase randomization in the microsphere suspension leads to photon bunching with a slower decay constant.

A single Lorentzian frequency distribution

$$S(f) = \frac{1}{\pi}\frac{\delta f/2}{(f-f_0)^2 + (\delta f/2)^2}, \tag{4}$$

around a centre frequency f_0 with a linewidth (FWHM) of δf leads via (2) and (3) to a normalized correlation function

$$g^{(2)}(\tau) = 1 + a e^{-|2\tau|/\tau_c} \quad \text{with} \quad \tau_c = 1/\delta f. \tag{5}$$

For a mixed spectral distribution $S(f)$, the intensity correlation function $g^{(2)}(\tau)$ can be obtained in a similar way. If the two contributions from blackbody and laser light are assumed to be mutually incoherent, the spectral power densities $S_B(f)$ and $S_L(f)$ can be added,

$$S(f) = S_B(f) + S_L(f), \tag{6}$$

and the resulting intensity correlation is given by

$$g^{(2)}(\tau) = 1 + |g^{(1)}(\tau)|^2 = 1 + \left|\mathcal{F}^{-1}[S_B(f)] + \mathcal{F}^{-1}[S_L(f)]\right|^2, \tag{7}$$

UNCORRECTED PROOF

with $\mathcal{F}^{-1}$ indicating the inverse Fourier transform. Assuming now two Lorentzian distributions $S_B(f)$ and $S_L(f)$ according to equation (4) with amplitudes a_L, a_B, coherence times τ_B, τ_L, and centre frequencies f_L, f_b, respectively, the Fourier transformation can easily be carried out, leading to

$$\begin{aligned} g^{(2)}(\tau) &= 1 + \left|a_B e^{-|\tau|/\tau_B} + a_L e^{-|\tau|/\tau_L}\right|^2 \\ &= 1 + a_B^2 e^{-|2\tau|/\tau_B} + a_L^2 e^{-|2\tau|/\tau_L} \\ &\quad + 2\cos[2\pi(f_L - f_B)\tau]\, a_B a_L\, e^{-|\tau|(1/\tau_B + 1/\tau_L)}. \end{aligned} \quad (8)$$

For $f_L = f_B$, the oscillating term vanishes, and equation (8) becomes a sum of three exponential decays on the top of $g^{(2)} = 1$ that can readily explain the correlation function in Fig. 3. There, the decay for large τ is dominated by the larger coherence time τ_L. The small peak near $\tau = 0$ is a combination of two fast decays, one given by the correlation of the blackbody contribution alone, the other one by the mixed term with about twice the decay time for $\tau_L \gg \tau_B$. A fit of the observed correlation function to the model (8) over photoevent separations of $-2\,\text{ns} < \tau < 96\,\text{ns}$ leads to $\tau_B = 0.39 \pm 0.03$ ns, $\tau_L = 49.0 \pm 2.3$ ns, $a_B = 0.36 \pm 0.02$ and $a_L = 0.452 \pm 0.004$. However, the relatively large reduced variance $\chi^2_{red} = 1.26$ indicates that model (8) is too simple and does not capture the oscillatory contributions in the measured $g^{(2)}$ visible in Fig. 3(b). The long coherence time corresponds to a linewidth of $\delta f = 1/\tau_L \approx 20$ MHz, comparable to the ones predicted for natural stellar lasers.

The described technique thus allows linewidth measurements of extremely narrow spectral lines, limited only by the ability to record a sufficiently large number of photons to construct a coincidence histogram. The upper bound of a linewidth measurement with this technique is given by the time resolution of the photodetectors and time-tagging mechanism (in our case a few GHz). However, the phase uncertainty of $g^{(1)}(\tau)$, if inferred from $g^{(2)}(\tau)$ in (2), requires further assumptions for a direct reconstruction of a spectrum via (3).

6 IDENTIFYING COHERENT LIGHT

In the second experiment, we try to identify the presence of coherent laser emission by a quantitative evaluation of the photobunching signature $g^{(2)}(\tau = 0)$. For this, we remove the microsphere suspension and record the temporal correlation measurement for different admixture levels of attenuated laser radiation to a blackbody radiation background of about 3×10^4 photoevents s^{-1} after the filter stack. Assuming a Lorentzian spectral distribution (4), the fit of the observed second-order correlation leads to a coherence time $\tau_c = 0.31 \pm 0.01$ ns in agreement with τ_B obtained from the fit in the first experiment.

The results are shown in Fig. 4. Without any laser light contribution, a detector-limited blackbody temporal bunching signature of approximately $g^{(2)}(0) = 1.5$ is observed, compatible with the transmission bandwidth around 3.2 GHz of the etalon stack at λ_L central wavelength and the timing jitter of the APD (Tan et al. 2016).

For a weak laser contribution ($\approx 10^4$ photoevents s^{-1}) on top of a blackbody background, the temporal photon bunching signal is reduced to $g^{(2)}(0) \approx 1.2$, indicating a subthermal photon bunching signature. This means that even the presence of small contributions of coherent light is revealed by the reduction of the thermal photon bunching signature expected from the filtered blackbody component.

For the third trace in Fig. 4, the laser light contribution is over two orders of magnitude stronger than the filtered blackbody contribution, corresponding to the power ratio used to obtain the spectrum in Fig. 2. The timing correlation appears constant within the

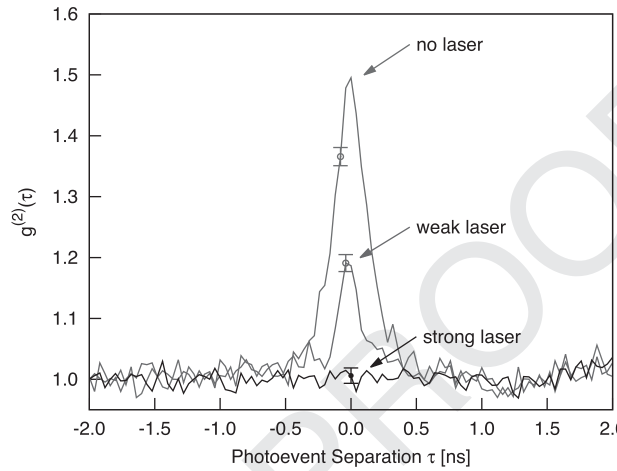

COLOUR ONLINE, B&W IN PRINT

Figure 4. Temporal photodetection correlations for different ratios of coherent laser and filtered blackbody radiation: all measurements have a blackbody contribution of approximately 3×10^4 photoevents s^{-1}. For the 'strong laser' trace, the laser contributed about 6×10^6 photoevents s^{-1}, for the 'weak laser' trace about 3×10^4 photoevents s^{-1}. For reference, the photodetection correlations of filtered blackbody radiation without any laser light is also shown. Each measurement accumulated 10^6 coincidence photoevents with -3.1 ns $< \tau <$ 3.3 ns into 40-ps-wide bins to allow for direct comparison of the resulting histograms. The error bars reflect Poissonian counting statistics and are representative for all time differences. Fitting the 'no laser' trace to model (5) leads to a coherence time $\tau_c = 0.31 \pm 0.01$ ns and to $\tau_c = 0.26 \pm 0.03$ ns for the trace with a weak laser.

statistical uncertainty, without an observable temporal photon bunching signature from the blackbody contribution.

The last trace resembles a typical photodetection correlation observed among the photodetectors exposed to wideband radiation, like in the traditional experiments of Hanbury-Brown & Twiss (1958), but with a significant difference. Since the optical bandwidth of the detected radiation is narrower than the inverse detector timing uncertainty, the *reduction* of a photobunching signal can be interpreted as a signature of a light source with sub-thermal statistics, e.g. due to contributions of coherent light from a lasing mechanism.

7 CONSIDERATIONS FOR SPECTROSCOPY OF ASTROPHYSICAL CANDIDATES

Precision spectroscopy of astronomical objects is often limited by the signal-to-noise ratio (SNR) of a particular technique. To compare the photocorrelation spectroscopy with other techniques, we consider the SNR of temporal intensity interferometry due to propagated Poissonian photon statistics for a narrow-band emission line as described by Hanbury-Brown (1974) and Malvimat et al. (2013):

$$\text{SNR} = \tau_c \frac{r}{2} V(b)^2 \sqrt{\frac{\Delta T}{2\Delta t}}\,. \quad (9)$$

In this expression, τ_c is the coherence time of the emission line with a lower bound provided by the spectral bandpass, r is the photodetection rate, ΔT is the overall measurement duration, Δt is the electronic resolution constrained by the photodetectors and $V(b)$ is the spatial visibility over baseline separation b, which approaches $V = 1$ for a telescope aperture much smaller than the transverse stellar coherence length.

The observed visible emission lines from the Weigelt Blobs B, C and D in the η Car system have intensities of the order of 10^4

UNCORRECTED PROOF

photons m^{-2} Mehner et al. 2010; Dravins & Germanà 2008).
Q9 To achieve an SNR of three with the spectral filtering technique described in this paper with a 3 GHz bandpass and detectors with 40 ps timing jitter, collecting starlight with a telescope of about 0.4 m aperture would require an observation time of approximately 6 h. In contrast, using a conventional interference filter with 1 nm bandpass would correspondingly increase the telescope aperture to about 7 m for the same SNR in 6 h.

While tuning of the etalons by temperature leads to a very good short-term stability for the pre-filters, it is still fast enough (i.e. within a few minutes) to account for time-dependent Doppler shifts of about 0.7 GHz light in the visible range due to the daily motion of the earth with respect to an astronomical object, or about 50 GHz due to the Earth's motion around the Sun.

8 SUMMARY

Time-resolved second-order correlation spectroscopy was used to identify the presence of very narrow-band light on a thermal background. The linewidth of pseudo-thermal light could be determined that was generated by phase-randomization in a multiple scattering process similar to light from an ensemble of emitters without a fixed phase relationship, like a gas cloud excited by a nearby star. Temporal intensity interferometry offers a spectral resolution of at least a few 10 MHz for emission lines, exceeding by far that of contemporary astrophysical spectrographs.

Also, an identification of sub-thermal photon statistics can be carried out with the presented technique, indicating a possible optical lasing mechanism, and therefore help to better understand the very narrow spectral features of stellar light sources even in the presence of a strong blackbody radiation background.

ACKNOWLEDGEMENTS

Q10 We acknow the support of this work by the National Research Foundation and the Ministry of Education in Singapore, partly through the Academic Research Fund MOE2012-T3-1-009.

REFERENCES

Arecchi F. T., 1965, Phys. Rev. Lett., 15, 912
Becker W., 2005, Advanced Time-Correlated Single Photon Counting Techniques. Springer-Verlag, Berlin
Dravins D., Germanà C., 2008, in Phelan D., Ryan O., Shearer A., eds, The Universe At Sub-Second Timescales. Am. Inst. Phys., New York, p. 284
Dravins D., Lagadec T., 2014, in Rajagopal J. K., Creech-Eakman M. J., Malbet F., eds, Proc. SPIE Conf. Ser. Vol. 9146, Optical and Infrared Interferometry IV. SPIE, Bellingham, p. 91460Z
Dravins D., Lagadec T., Nuñez P. D., 2015, Nature Commun., 6, 6852
Estes L. E., Narducci L. M., Tu A., 1971, J. Opt. Soc. Am., 61, 1301
Fried D. L., 1967, Proc. IEEE, Q11
Gal-Yam A. et al., 2014, Nature, 50 Q12
Glauber R., 1963, Phys. Rev., 131, 2766
Griest K., Whitmore J. B., Wolfe A. M., Prochaska J. X., Howk J. C., Marcy G. W., 2010, ApJ, 708, 158
Hale D. D. S. et al., 2000, ApJ, 537 Q13
Hamann F., DePoy D. L., 1994, ApJ, 422, 626
Hanbury-Brown R., 1974, The Intensity Interferometer: Its Application to Astronomy. Taylor & Francis/Halsted Press, London/New York
Hanbury-Brown R., Twiss R. Q., 1956, Nature, 178, 1046
Hanbury-Brown R., Twiss R. Q., 1958, Proc. R. Soc. A, 243, 291
Hard R., Zeh R., Allen R. D., 1977, J. Cell Sci., 23, 335
Johansson S., Letokhov V. S., 2005, New Astron., 10, 361
Khinchin A., 1934, Math. Ann., 109, 604
Loewenstein E. V., 1966, Appl. Opt., 5, 845
Malvimat V., Wucknitz O., Saha P., 2013, MNRAS, 437, 798
Mandel L., Wolf E., 1975, J. Opt. Soc. Am., 65 Q14
Mandel L., Wolf E., 1995, Optical Coherence and Quantum Optics. Cambridge Univ. Press, Cambridge
Martienssen W., Spiller E., 1964, Am. J. Phys., 32, 919
Mehner A., Davidson K., Ferland G. J., Humphreys R. M., 2010, ApJ, 710, 729
Menzel D. H., 1970, in Groth H. G., Wellmann P., eds, Proc. IAU Symp. 332, Spectrum Formation in Stars with Steady-State Extended Atmospheres. Munich, Germany, p. 134
Murphy M. T. et al., 2007, MNRAS 839
Pike E. R., 2010, JEOS:RP, 5, 10047 Q15
Sakai H., Vanasse G. A., Forman M. L., 1968, J. Opt. Soc. Am., 58, 84
Saleh B., 1978, Photoelectron Statistics: With Applications to Spectroscopy and Optical Communication. Springer-Verlag, Berlin
Scarl D. B., 1966, Phys. Rev. Lett., 17, 663
Scarl D. B., 1968, Phys. Rev., 175, 1661
Shaklan S., Roddier F., 1988, Appl. 27, 2334
Siegman A. E., 1966, Proc. IEEE, 54 Q16
Sonnabend G., Wirtz D., Vetterle V., Schieder R., 2005, A&A, 435, 1181
Tan P. K., Yeo G. H., Poh H. S., Chan A. H., Kurtsiefer C., 2014, ApJ, 789, L10
Tan P. K., Chan A. H., Kurtsiefer C., 2016, MNRAS, 457, 4291
Varshni Y. P., Nasser R. M., 1986, Ap&SS, 125, 341
Weaver H., Williams D. R., Dieter N., Lum W., 1965, Nature, 208, 29
Wiener N., 1930, Acta Math., 55, 117
Wilken T. et al., 2012, Nature, 485, 611
Zethsson T., Johansson S., Hartman H., Gull T. R., 2012, A&A, 540 Q17

This paper has been typeset from a TEX/LATEX file prepared by the author.

UNCORRECTED PROOF

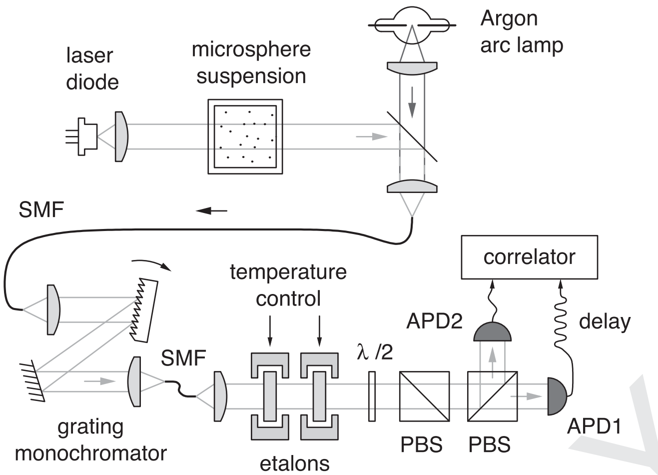

Figure 1. Experimental set-up. Light from a laser diode ($\lambda_L = 513.8$ nm) is Doppler-broadened by passing through a suspension of microspheres (0.2 μm diameter), combined with light from an Argon arc lamp on a microscope slide, and coupled into a single-mode optical fibre (SMF). The bottom part shows the analysis system, consisting of a grating monochromator and a temperature-tuned etalon pair to select a 3.2-GHz-wide spectral window around 513.8 nm from the composite light. Temporal photon pair correlations are recorded to identify different light contributions. PBS: polarizing beam splitter; $\lambda/2$: half wave plate; APD: single-photon avalanche photodetectors.

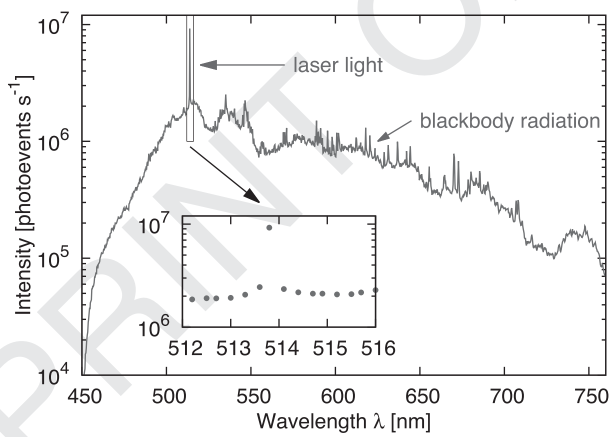

Figure 2. Spectrum of the test light source in Fig. 1 without Doppler broadening. The broad background over the whole visible range resembles blackbody radiation at an effective temperature of $T = 6000$ K, while the inset shows the unresolved spectrum around the laser line. The resolution of the spectrometer is about 0.12 nm.

PRINT ONLY

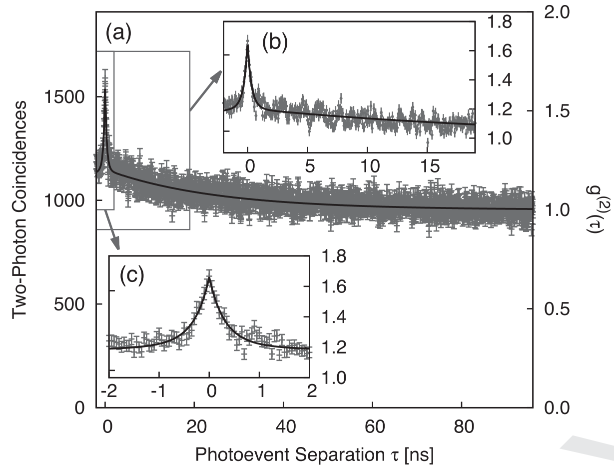

Figure 3. (a) The two-photoevent coincidence histogram from filtered blackbody radiation with a Doppler- broadened laser light contribution shows two exponential decays on a short and a long time-scale (bin width 50 ps). The solid line shows a fit of the data to model (8), assuming $f_B = f_L$. The two zooms show (b) an oscillatory behaviour on top of the slow decay and (c) a good match between the fit and measured data for the filtered blackbody radiation on a short time-scale.

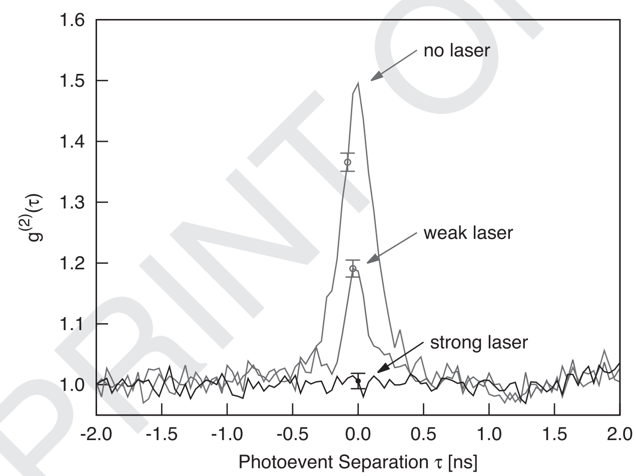

Figure 4. Temporal photodetection correlations for different ratios of coherent laser and filtered blackbody radiation: all measurements have a blackbody contribution of approximately 3×10^4 photoevents s^{-1}. For the 'strong laser' trace, the laser contributed about 6×10^6 photoevents s^{-1}, for the 'weak laser' trace about 3×10^4 photoevents s^{-1}. For reference, the photodetection correlations of filtered blackbody radiation without any laser light is also shown. Each measurement accumulated 10^6 coincidence photoevents with -3.1 ns $< \tau < 3.3$ ns into 40-ps-wide bins to allow for direct comparison of the resulting histograms. The error bars reflect Poissonian counting statistics and are representative for all time differences. Fitting the 'no laser' trace to model (5) leads to a coherence time $\tau_c = 0.31 \pm 0.01$ ns and to $\tau_c = 0.26 \pm 0.03$ ns for the trace with a weak laser.

PRINT ONLY

List of astronomical key words (Updated on 2017 March)

This list is common to *Monthly Notices of the Royal Astronomical Society, Astronomy and Astrophysics*, and *The Astrophysical Journal*. In order to ease the search, the key words are subdivided into broad categories. No more than *six* subcategories altogether should be listed for a paper.

The subcategories in boldface containing the word 'individual' are intended for use with specific astronomical objects; these should never be used alone, but always in combination with the most common names for the astronomical objects in question. Note that each object counts as one subcategory within the allowed limit of six.

The parts of the key words in italics are for reference only and should be omitted when the keywords are entered on the manuscript.

General
editorials, notices
errata, addenda
extraterrestrial intelligence
history and philosophy of astronomy
miscellaneous
obituaries, biographies
publications, bibliography
sociology of astronomy
standards

Physical data and processes
acceleration of particles
accretion, accretion discs
asteroseismology
astrobiology
astrochemistry
astroparticle physics
atomic data
atomic processes
black hole physics
chaos
conduction
convection
dense matter
diffusion
dynamo
elementary particles
equation of state
gravitation
gravitational lensing: micro
gravitational lensing: strong
gravitational lensing: weak
gravitational waves
hydrodynamics
instabilities
line: formation
line: identification
line: profiles
magnetic fields
magnetic reconnection
(magnetohydrodynamics) MHD
masers
molecular data
molecular processes
neutrinos
nuclear reactions, nucleosynthesis, abundances
opacity
plasmas
polarization
radiation: dynamics
radiation mechanisms:general
radiation mechanisms: non-thermal
radiation mechanisms: thermal
radiative transfer
relativistic processes
scattering
shock waves
solid state: refractory
solid state: volatile
turbulence
waves

Astronomical instrumentation, methods and techniques
atmospheric effects
balloons
instrumentation: adaptive optics
instrumentation: detectors
instrumentation: high angular resolution
instrumentation: interferometers
instrumentation: miscellaneous
instrumentation: photometers
instrumentation: polarimeters
instrumentation: spectrographs
light pollution
methods: analytical
methods: data analysis
methods: laboratory: atomic
methods: laboratory: molecular
methods: laboratory: solid state
methods: miscellaneous
methods: numerical
methods: observational
methods: statistical
site testing
space vehicles
space vehicles: instruments
techniques: high angular resolution
techniques: image processing
techniques: imaging spectroscopy
techniques: interferometric
techniques: miscellaneous
techniques: photometric
techniques: polarimetric
techniques: radar astronomy
techniques: radial velocities
techniques: spectroscopic
telescopes

Astronomical data bases
astronomical data bases: miscellaneous
atlases
catalogues
surveys
virtual observatory tools

Astrometry and celestial mechanics
astrometry
celestial mechanics
eclipses
ephemerides
occultations
parallaxes
proper motions
reference systems
time

The Sun
Sun: abundances
Sun: activity
Sun: atmosphere
Sun: chromosphere
Sun: corona
Sun: coronal mass ejections (CMEs)
Sun: evolution
Sun: faculae, plages
Sun: filaments, prominences
Sun: flares
Sun: fundamental parameters
Sun: general
Sun: granulation
Sun: helioseismology
Sun: heliosphere
Sun: infrared
Sun: interior
Sun: magnetic fields
Sun: oscillations
Sun: particle emission
Sun: photosphere
Sun: radio radiation
Sun: rotation
(Sun:) solar–terrestrial relations
(Sun:) solar wind
(Sun:) sunspots
Sun: transition region
Sun: UV radiation
Sun: X-rays, gamma-rays

Planetary systems
comets: general

comets: individual: . . .
Earth
interplanetary medium
Kuiper belt: general

Kuiper belt objects: individual: . . .
meteorites, meteors, meteoroids
minor planets, asteroids: general

minor planets, asteroids: individual: . . .
Moon
Oort Cloud
planets and satellites: atmospheres
planets and satellites: aurorae
planets and satellites: composition
planets and satellites: detection
planets and satellites: dynamical evolution and stability
planets and satellites: formation
planets and satellites: fundamental parameters
planets and satellites: gaseous planets
planets and satellites: general

planets and satellites: individual: . . .
planets and satellites: interiors
planets and satellites: magnetic fields
planets and satellites: oceans
planets and satellites: physical evolution
planets and satellites: rings
planets and satellites: surfaces
planets and satellites: tectonics
planets and satellites: terrestrial planets
planet–disc interactions
planet–star interactions
protoplanetary discs
zodiacal dust

Stars
stars: abundances
stars: activity
stars: AGB and post-AGB
stars: atmospheres
(stars:) binaries *(including multiple)*: close
(stars:) binaries: eclipsing
(stars:) binaries: general
(stars:) binaries: spectroscopic
(stars:) binaries: symbiotic
(stars:) binaries: visual
stars: black holes
(stars:) blue stragglers
(stars:) brown dwarfs
stars: carbon
stars: chemically peculiar
stars: chromospheres
(stars:) circumstellar matter
stars: coronae
stars: distances
stars: dwarf novae
stars: early-type
stars: emission-line, Be
stars: evolution
stars: flare
stars: formation
stars: fundamental parameters
(stars:) gamma-ray burst: general
(stars:) **gamma-ray burst: individual: . . .**
stars: general
(stars:) Hertzsprung–Russell and colour–magnitude diagrams
stars: horizontal branch
stars: imaging
stars: individual: . . .
stars: interiors

stars: jets
stars: kinematics and dynamics
stars: late-type
stars: low-mass
stars: luminosity function, mass function
stars: magnetars
stars: magnetic field
stars: massive
stars: mass-loss
stars: neutron
(stars:) novae, cataclysmic variables
stars: oscillations *(including pulsations)*
stars: peculiar *(except chemically peculiar)*
(stars:) planetary systems
stars: Population II
stars: Population III
stars: pre-main-sequence
stars: protostars
(stars:) pulsars: general
(stars:) **pulsars: individual: . . .**
stars: rotation
stars: solar-type
(stars:) starspots
stars: statistics
(stars:) subdwarfs
(stars:) supergiants
(stars:) supernovae: general
(stars:) **supernovae: individual: . . .**
stars: variables: Cepheids
stars: variables: Scuti
stars: variables: general
stars: variables: RR Lyrae
stars: variables: S Doradus
stars: variables: T Tauri, Herbig Ae/Be
(stars:) white dwarfs
stars: winds, outflows
stars: Wolf–Rayet

Interstellar medium (ISM), nebulae
ISM: abundances
ISM: atoms
ISM: bubbles
ISM: clouds
(ISM:) cosmic rays
(ISM:) dust, extinction
ISM: evolution
ISM: general
(ISM:) HII regions
(ISM:) Herbig–Haro objects

ISM: individual objects: . . .
(except planetary nebulae)
ISM: jets and outflows
ISM: kinematics and dynamics
ISM: lines and bands
ISM: magnetic fields
ISM: molecules
(ISM:) photodissociation region (PDR)
(ISM:) planetary nebulae: general
(ISM:) **planetary nebulae: individual: . . .**
ISM: structure
ISM: supernova remnants

The Galaxy
Galaxy: abundances
Galaxy: bulge
Galaxy: centre
Galaxy: disc
Galaxy: evolution
Galaxy: formation
Galaxy: fundamental parameters
Galaxy: general
(Galaxy:) globular clusters: general
(Galaxy:) **globular clusters: individual: . . .**
Galaxy: halo
Galaxy: kinematics and dynamics
(Galaxy:) local interstellar matter
Galaxy: nucleus
(Galaxy:) open clusters and associations: general
(Galaxy:) **open clusters and associations: individual: . . .**
(Galaxy:) solar neighbourhood
Galaxy: stellar content
Galaxy: structure

Galaxies
galaxies: abundances
galaxies: active
(galaxies:) BL Lacertae objects: general
(galaxies:) **BL Lacertae objects: individual: . . .**
galaxies: bulges
galaxies: clusters: general

galaxies: clusters: individual: . . .
galaxies: clusters: intracluster medium
galaxies: distances and redshifts
galaxies: dwarf
galaxies: elliptical and lenticular, cD
galaxies: evolution
galaxies: formation
galaxies: fundamental parameters
galaxies: general
galaxies: groups: general

galaxies: groups: individual: . . .
galaxies: haloes
galaxies: high-redshift

galaxies: individual: . . .
galaxies: interactions
(galaxies:) intergalactic medium
galaxies: irregular
galaxies: ISM
galaxies: jets
galaxies: kinematics and dynamics
(galaxies:) Local Group
galaxies: luminosity function, mass function
(galaxies:) Magellanic Clouds
galaxies: magnetic fields
galaxies: nuclei
galaxies: peculiar
galaxies: photometry
(galaxies:) quasars: absorption lines
(galaxies:) quasars: emission lines
(galaxies:) quasars: general

(galaxies:) **quasars: individual: . . .**
(galaxies:) quasars: supermassive black holes
galaxies: Seyfert
galaxies: spiral
galaxies: starburst
galaxies: star clusters: general

galaxies: star clusters: individual: . . .
galaxies: star formation
galaxies: statistics
galaxies: stellar content
galaxies: structure

Cosmology
(cosmology:) cosmic background radiation
(cosmology:) cosmological parameters
(cosmology:) dark ages, reionization, first stars
(cosmology:) dark energy
(cosmology:) dark matter
(cosmology:) diffuse radiation
(cosmology:) distance scale
(cosmology:) early Universe
(cosmology:) inflation
(cosmology:) large-scale structure of Universe
cosmology: miscellaneous
cosmology: observations
(cosmology:) primordial nucleosynthesis
cosmology: theory

Resolved and unresolved sources as a function of wavelength
gamma-rays: diffuse background
gamma-rays: galaxies
gamma-rays: galaxies: clusters
gamma-rays: general
gamma-rays: ISM
gamma-rays: stars
infrared: diffuse background
infrared: galaxies
infrared: general
infrared: ISM
infrared: planetary systems
infrared: stars
radio continuum: galaxies
radio continuum: general
radio continuum: ISM
radio continuum: planetary systems
radio continuum: stars
radio continuum: transients
radio lines: galaxies
radio lines: general
radio lines: ISM
radio lines: planetary systems
radio lines: stars
submillimetre: diffuse background
submillimetre: galaxies
submillimetre: general
submillimetre: ISM
submillimetre: planetary systems
submillimetre: stars
ultraviolet: galaxies
ultraviolet: general
ultraviolet: ISM
ultraviolet: planetary systems
ultraviolet: stars
X-rays: binaries
X-rays: bursts
X-rays: diffuse background
X-rays: galaxies
X-rays: galaxies: clusters
X-rays: general
X-rays: individual: . . .
X-rays: ISM
X-rays: stars